# Guidance Control of a Small Unmanned Aerial Vehicle with a Delta Wing

**Shuichi TAJIMA⋆, Takuya AKASAKA⋆, Makoto KUMON⋆ and Kazuo OKABE†**
⋆: Kumamoto University, Japan
s.tajima@ick.mech.kumamoto-u.ac.jp, kumon@gpo.kumamoto-u.ac.jp
†: Sky Remote Inc., Japan

## Abstract

A small and light unmanned aerial vehicle (UAV) with a delta-shaped main wing called a kiteplane is considered in this paper. The UAV is suitable for ground observation because of its slow flying speed, which can be achieved due to its light weight and large main wing; however, the aircraft can be greatly disturbed by a control command (set point) update or a wind disturbance. In order to compensate for this problem, this paper proposes a "bank-and-turn" approach for path-following control based on nonlinear attitude control. The bank angle of the kiteplane is commanded so as to track the desired path, and the reference signal is designed using stability analysis. The results of a numerical simulation are also presented to validate the proposed approach.

## 1 Introduction

Rescue activities and surveillance missions in dangerous areas, such as those affected by natural disasters, are important in order to save victims and obtain important data. Those areas are not always easily accessible by ordinary means since the infrastructure (including the standard modes of transportation) can be severely damaged. Therefore, unmanned aerial vehicles (UAVs) are expected to be used because they are able to be operated remotely.

UAVs can be classified into two categories according to their configuration: fixed-wing UAVs and rotary-wing UAVs. Both types of UAVs have been studied actively (e.g., [Mueller and DeLaurier, 2001; Chao *et al.*, 2010]). Fixed-wing UAVs are efficient in terms of energy consumption since they can glide, but they normally fly rather fast, which is not suitable for measuring objects on the ground. On the other hand, rotary-wing UAVs such as helicopters are able to hover in one location, which provides the ability to capture terrain data but limits the endurance because of the high energy consumption. In this paper, a lightweight fixed-wing UAV with a large main wing that realizes a slow flight speed in order to compensate for the standard fixed-wing UAV drawbacks is considered for surveillance missions. This UAV is named a kiteplane because its main wing is made of cloth and has a delta triangle shape like a kite, as shown in Fig. 1.


Figure 1: Kiteplane

Nagata [Nagata *et al.*, 2004] proposed PID control for the kiteplane because of its simple dynamics, and the author [Kumon *et al.*, 2006] proposed a fuzzy-logic based nonlinear flight controller for waypoint tracking. These methods use the position of the aircraft to directly control its flight path without considering the attitude due to its stable dynamics. Although this approach succeeded at simplifying the controller structure, large attitude deviations could be triggered by set-point changes after the aircraft passed waypoints or by strong wind turbulence, which might lead to significant overshoot or oscillation.

In order to improve the flight-path-following perfor-

mance, this paper proposes realizing "bank-and-turn" for a straight line and a circular orbit using a roll angle controller with the nonlinear attitude control from the kiteplane proposed by Akasaka [Akasaka and Kumon, 2012].

The present paper is organized as follows: In the next section, the kiteplane and its dynamics are briefly introduced. Then, Sec. 3 first introduces Akasaka's controller, and the path-following controller is proposed. In order to validate the proposed approach, Sec. 4 shows the numerical simulation results, and the conclusions follow in (Sec. 5).

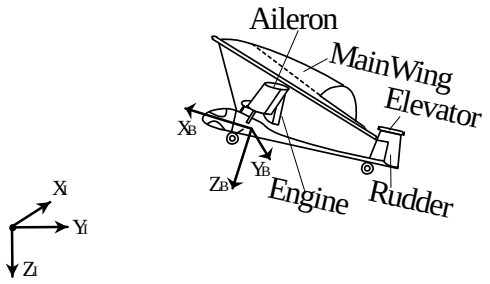


Figure 2: Inertial frame and body frame

## 2 Small UAV with Delta Wing: Kiteplane

### 2.1 Kiteplane

A kiteplane is a UAV that has a kite-like main wing in the shape of a delta, as shown in Fig. 1. The main wing is light and flexible because it is made of cloth, and the UAV is capable of carrying a large payload. The wing's flexibility provides safety and robustness if it crashes into the ground. The center of mass is located under the main wing, and the ailerons are attached at dihedral angles. The kiteplane's length, wingspan, and height are 1160 mm, 900 mm, and 2040 mm, respectively, and it weighs approximately 4.5 kg.

The kiteplane has three control surfaces: the ailerons, the elevator, and the rudder, and they are actuated by servomotors. The propeller that generates the thrust required to fly is driven by a brushless motor, and its rotational speed is controlled by a speed controller.

A global positioning system (GPS) is installed to measure the delta wing's position, and a three-dimensional accelerometer, a three-dimensional rate gyro, and a three-dimensional magnetometer are also installed to estimate the attitude of the aircraft. In this paper, it is assumed that the three-dimensional position, attitude and their time derivatives are available with respect to the inertial frame.

### 2.2 Dynamics of the Kiteplane

The dynamics of the kiteplane are presented in this subsection. It is assumed that the total aerodynamic force and torque can be modeled as a sum of the forces acting on the wings.

The frames considered in this paper are shown in Fig. 2, and the quantities with respect to the inertial frame and body frame are denoted by subscripts $_I$ and $_B$ when distinction is necessary.

The aerodynamic forces that affect the main wing, the ailerons, the elevator, and the rudder (with respect to the body frame) are denoted as $\boldsymbol{f_m}$, $\boldsymbol{f_a}$, $\boldsymbol{f_e}$, and $\boldsymbol{f_r}$, respectively, and the thrust generated by the propeller is indicated by $\boldsymbol{T}$ as in [Kumon *et al.*, 2006]. The aerodynamic parameters, such as the air speed and angle of attack, have nonlinear effects on those forces, and the forces affecting the ailerons, the elevator, and the rudder are also governed by control inputs since those wings are control surfaces.

The aerodynamic force on the elevator $\boldsymbol{f}_e$ with respect to the wing frame, which is the frame around the wing with its $-X$ and $Z$ axes in the drag and lift directions, respectively, is denoted as ${\boldsymbol{f_e}}^W$. In this paper, the following aerodynamic model is introduced:

$$ {\boldsymbol{f_e}}^W = \begin{bmatrix} -\frac{1}{2}\rho V^2 S_e C_D \\ 0 \\ \frac{1}{2}\rho V^2 S_e C_L \end{bmatrix}, \tag{1} $$

where $\rho$, $V$, $S_e$, $C_L$, and $C_D$ represent the air density, flow speed, elevator area, lift coefficient, and drag coefficient, respectively. $C_L$ and $C_D$ are considered linear functions of the control input to the elevator. ${\boldsymbol{f_e}}^W$ is transformed to the body frame to compute $\boldsymbol{f_e}$. Other aerodynamic terms, $\boldsymbol{f_m}$, $\boldsymbol{f_a}$, and $\boldsymbol{f_r}$, are also modeled in a similar manner and then summed up to obtain $\boldsymbol{f_B}$, which is shown below. Since the flow speed $V$ can be computed from the wind and the velocity of the aircraft itself, which is a part of the system state, the model contains nonlinear terms with respect to the state of the system. It is considered possible for the magnitude of the thrust $|\boldsymbol{T}|$ to be commanded directly since the rotation speed of the propeller for the real platform is well controlled due to an inner-loop speed controller with a high-power electric motor.

Considering the UAV as a rigid body, the motion equation with respect to the center of mass can be given as follows:

$$ m\frac{d^2}{dt^2}\begin{bmatrix} x_I & y_I & z_I \end{bmatrix}^{\mathrm{T}} = \boldsymbol{f_I}, \tag{2} $$

$$ \boldsymbol{I_B}\frac{d}{dt}\boldsymbol{\omega_B} + \boldsymbol{\omega_B} \times \boldsymbol{I_B}\boldsymbol{\omega_B} = \boldsymbol{n_B}, \tag{3} $$

where

$$\begin{aligned}\tilde{\boldsymbol{f_I}} &= \boldsymbol{q} \odot \tilde{\boldsymbol{f_B}} \odot \boldsymbol{q}^* \\ &= \boldsymbol{q} \odot \left(\tilde{\boldsymbol{f_m}} + \tilde{\boldsymbol{f_a}} + \tilde{\boldsymbol{f_e}} + \tilde{\boldsymbol{f_r}} + \tilde{\boldsymbol{T}}\right) \odot \boldsymbol{q}^* \\ \boldsymbol{n_B} &= \boldsymbol{l_m} \times \boldsymbol{f_m} + \boldsymbol{l_a} \times \boldsymbol{f_a} + \boldsymbol{l_e} \times \boldsymbol{f_e} \\ &\quad + \boldsymbol{l_r} \times \boldsymbol{f_r} + \boldsymbol{l_T} \times \boldsymbol{T}.\end{aligned}$$

Here, $x_I$, $y_I$, and $z_I$ indicate the position of the body, and $\boldsymbol{\omega_B}$ represents the angular velocity. The attitude is represented by a quaternion $\boldsymbol{q}$, and $\odot$ represents the multiplication of quaternions. $\boldsymbol{f_I}$ and $\boldsymbol{f_B}$ represent the forces acting on the center of mass with respect to the body frame and the inertial frame, respectively, and $\boldsymbol{n_B}$ denotes the torque on the body. The translation between $\boldsymbol{f_I}$ and $\boldsymbol{f_B}$ can be given by using a quaternion as shown above, and $\tilde{\boldsymbol{x}}$ represents a quaternion with the vector $\boldsymbol{x}$ for its imaginary part (*i.e.,* $\tilde{\boldsymbol{x}} = \left[0, \boldsymbol{x}^T\right]^T$), and $^*$ shows the conjugate operation of the quaternion. $m$ and $\boldsymbol{I_B}$ represent the mass of the body and the inertial matrix, respectively. $\boldsymbol{l_m}$, $\boldsymbol{l_a}$, $\boldsymbol{l_e}$, $\boldsymbol{l_r}$, and $\boldsymbol{l_T}$ represent the position of the aerodynamic forces acting on the wings. Further details of the quaternion operations can be found in [Murray *et al.*, 1994].

In this paper, the attitude is represented by the quaternion, and its dynamics are given as follows:

$$\frac{d}{dt}\boldsymbol{q} = \frac{1}{2}\tilde{\boldsymbol{\omega_I}} \odot \boldsymbol{q} = \frac{1}{2}\boldsymbol{q} \odot \tilde{\boldsymbol{\omega_B}} \tag{4}$$

Let the state of the system be represented by $(x_I, y_I, z_I, \frac{d}{dt}x_I, \frac{d}{dt}y_I, \frac{d}{dt}z_I, \boldsymbol{q}, \boldsymbol{\omega_B})$. Recalling the fact that $\boldsymbol{f_B}$ and $\boldsymbol{n_B}$ can be computed if the state and control inputs are given, the evolution of the system can be obtained by the dynamics (2), (3), and (4).

## 3 Guidance Control of Kiteplane

The proposed guidance controller consists of inner-loop attitude control and outer-loop path-following control. In the following subsections, the inner-loop attitude controller proposed by Akasaka [Akasaka and Kumon, 2012] is shown first, and then, the path-following controller for straight-line reference paths and circular orbits is proposed, which is the main contribution of this paper.

### 3.1 Attitude control

Attitude control for a kiteplane was proposed by Akasaka [Akasaka and Kumon, 2012], and this subsection briefly introduces the method.

Based on the dynamics shown above, the dynamics of the attitude subsystem can be represented as follows:

$$\begin{aligned}\dot{\tilde{q}} &= \frac{1}{2}\tilde{q} \cdot \tilde{\omega}_B \\ \dot{\boldsymbol{\omega}}_{\boldsymbol{B}} &= \boldsymbol{I_B}^{-1}\left(\boldsymbol{n_B} - \boldsymbol{\omega_B} \times \boldsymbol{I_B}\boldsymbol{\omega_B}\right)\end{aligned} \tag{5}$$

The attitude and its reference are represented by quaternions, and they are denoted by $\boldsymbol{q}$ and $\boldsymbol{q_d}$, respectively. The reference angular velocity is defined as $\boldsymbol{\omega_{dB}}$, and the following holds as in (4):

$$\frac{d}{dt}\boldsymbol{q_d} = \frac{1}{2}\boldsymbol{q_d} \odot \tilde{\boldsymbol{\omega_{dB}}}.$$

The real and imaginary parts of those quaternions are denoted as

$$\boldsymbol{q} = \begin{bmatrix} t \\ \boldsymbol{p} \end{bmatrix}, \quad \boldsymbol{q_d} = \begin{bmatrix} t_d \\ \boldsymbol{p_d} \end{bmatrix}$$

and the attitude error denoted by $\boldsymbol{e_q}$ is defined as

$$\boldsymbol{e_q} \triangleq \boldsymbol{q} - \boldsymbol{q_d} = \begin{bmatrix} e_t \\ \boldsymbol{e_p} \end{bmatrix}.$$

Here, $\boldsymbol{n_B}$ is the quantity that primarily governs the attitude motion, and it is assumed that $\boldsymbol{n_B}$ can be modeled as

$$\boldsymbol{n}_B = \boldsymbol{G}\boldsymbol{u} + \boldsymbol{n_d}, \tag{6}$$

where $\boldsymbol{u}$ represents the control input vector, and $\boldsymbol{G}$ and $\boldsymbol{n_d}$ represent a non-singular known matrix and a bounded disturbance term, respectively. The difference between $\tilde{\boldsymbol{\omega_B}}$ and $\tilde{\boldsymbol{\omega_{dB}}}$ is defined as $\tilde{\boldsymbol{\nu}}$, and its imaginary part is defined as $\boldsymbol{\nu_p}$ as above, or

$$\boldsymbol{\nu} \triangleq \tilde{\boldsymbol{\omega_B}} - \tilde{\boldsymbol{\omega_{dB}}} = \begin{bmatrix} 0 \\ \boldsymbol{\nu_p} \end{bmatrix}.$$

An augmented reference signal denoted by $\boldsymbol{\xi}$ is defined as

$$\boldsymbol{\xi} = \boldsymbol{\omega_{dB}} - \boldsymbol{K_q}(-e_t\boldsymbol{p} + t\boldsymbol{e_p} + \boldsymbol{e_p} \times \boldsymbol{p}), \tag{7}$$

where $\boldsymbol{K_q}$ shows a positive symmetric matrix. Since $\boldsymbol{\xi}$ is differentiable, the control input $\boldsymbol{u}$ is defined as

$$\boldsymbol{u} = \boldsymbol{G}^{-1}\left\{-\boldsymbol{K_\nu}\boldsymbol{\nu} + \boldsymbol{\omega_B} \times \boldsymbol{I_B}\boldsymbol{\omega_B} + \boldsymbol{I_B}\dot{\boldsymbol{\xi}}\right\}, \tag{8}$$

where $\boldsymbol{K_\nu}$ is a positive symmetric matrix. The control input (8) enables the UAV to follow the desired attitude, which can be shown as follows:

Consider a positive scalar function of $\boldsymbol{e_q}$ as $V_q = \boldsymbol{e_q}^{\mathrm{T}}\boldsymbol{e_q}$, and a simple calculation shows that the time derivative of $V_q$ can be evaluated as

$$\dot{V}_q = (-e_t\boldsymbol{p} + t\boldsymbol{e_p} + \boldsymbol{e_p} \times \boldsymbol{p})^T\boldsymbol{\nu_p}.$$

If $\boldsymbol{\nu_p}$ is equal to or very close to $-\boldsymbol{K_q}(-e_t\boldsymbol{p}+t\boldsymbol{e_p}+\boldsymbol{e_p}\times\boldsymbol{p})$, then $\boldsymbol{e_q}$ converges close to the origin. In order to validate the above, another scalar positive function is introduced,

$$V_\nu = \frac{1}{2}\boldsymbol{e_\nu}^T\boldsymbol{I_B}\boldsymbol{e_\nu} \tag{9}$$

where

$$\boldsymbol{e_\nu} \triangleq \nu_p - (-\boldsymbol{K_q}(-e_t\boldsymbol{p} + t\boldsymbol{e_p} + \boldsymbol{e_p} \times \boldsymbol{p})).$$

Using the input (8), differentiating $V_\nu$ with respect to time leads to

$$\dot{V_\nu} \leq \boldsymbol{e_\nu^T n_d} - k_\nu |\boldsymbol{e_\nu}|^2, \tag{10}$$

where $k_\nu$ shows the minimum eigenvalue of $\boldsymbol{K_\nu}$. Since $\boldsymbol{n_d}$ is bounded, $\boldsymbol{e_\nu}$ will converge sufficiently close to the origin by selecting a large enough $k_\nu$.

### 3.2 Guidance control

In this paper, the path to follow is mainly considered in two-dimensional space, and the altitude is controlled independently. The altitude controller is shown first, and then, the main path-following controller is proposed.

**Altitude control**

The objective for the altitude control described in this paper is to maintain a constant height during flight. The current altitude, its reference, and the reference altitude change rate are denoted by $z$, $z_d$, and $v_{zd}$, respectively. Taking the limit of the control input range into account, $v_{zd}$ is defined as

$$v_{zd} = -\tanh\{k_z(z - z_d)\}, \tag{11}$$

where $k_z$ represents a positive constant. Since the altitude is primarily dominated by thrust, the altitude controller is defined as follows:

$$|\boldsymbol{T}| = -k_t(\frac{d}{dt}z - v_{zd}) + T_0, \tag{12}$$

where $k_t$ and $T_0$ represent a positive constant feedback gain and the trim input for the throttle, respectively.

**Path-following control**

It is common to approximate a UAV as a point mass and to limit the path to follow straight lines and circles or arcs since the well-known Dubin's model [Dubins, 1957] can achieve the shortest path between two given points by using a combination of those sections. Therefore, the path-following control of a straight line and a circular orbit is considered in this paper.

Since the inner-loop controller controls the attitude, the roll angle, or bank, is considered as the input to control the position of the UAV, and the angle is denoted by $\theta$. The heading angle is also controlled to converge to the desired direction, but its transient response may affect the path-following performance. In order to take this effect into account, the current heading angle and the desired angle, which are denoted as $\alpha$ and $\alpha_d$, respectively, are also considered. Because of the attitude controller, it can be assumed that $\alpha - \alpha_d \approx 0$.

Point mass model

As the simplest model, the UAV dynamics are approximated by a point mass, and the motion equation can be given as follows:

$$m\frac{d^2}{dt^2}x_I = T\cos\alpha + L\sin\theta\sin\alpha - D\cos\alpha \tag{13}$$

$$m\frac{d^2}{dt^2}y_I = T\sin\alpha - L\sin\theta\cos\alpha - D\sin\alpha, \tag{14}$$

where $L$ and $D$ denote the lift and drag force affecting the UAV.

Circle case

Denote the reference circle radius as $r_d$ and the distance from the center to the current UAV position as $r$. Without loosing the generality, the center of the reference circle is assumed to be the origin of the coordinate frame. Defining the error $e_r \triangleq r - r_d$, the control objective can be defined to make $e_r \to 0$ as $t \to \infty$. $\alpha_d$ is given as the direction tangential to the reference path in this case.

Let $k_1$ and $k_2$ represent the appropriate positive feedback gains, and assume $\cos(\alpha - \alpha_d) \neq 0$. The bank angle $\theta$ is defined as follows:

$$\sin\theta = \frac{k_1 e_r + k_2\dot{r} + (T - D)\sin(\alpha - \alpha_d) + mr\frac{d}{dt}\alpha_d^{\,2}}{L\cos(\alpha - \alpha_d)}, \tag{15}$$

when the right hand side is within the range of $-1$ to 1; otherwise, $\theta$ will be selected to clip to $-\pi$ or $\pi$. The reference roll angle (15) can be validated as follows.

The motion equations (13) and (14) can be rewritten with respect to the radial direction as

$$m\frac{d^2}{dt^2}r = (T - D)\sin(\alpha - \alpha_d) - L\sin\theta\cos(\alpha - \alpha_d) + mr\frac{d}{dt}\alpha_d^{\,2}. \tag{16}$$

Introducing a small positive constant $\epsilon$, the scalar function $V_r$ is defined as

$$V_r = \frac{k_1 + \epsilon k_2}{2}e_r^2 + \frac{m}{2}(\frac{d}{dt}e_r)^2 + \epsilon m e_r\frac{d}{dt}e_r. \tag{17}$$

When $\epsilon$ is sufficiently small, it is obvious that $V_r$ is greater than or equal to 0, and there exists a positive constant $B_1$ that satisfies the following inequality:

$$V_r \geq B_1\left\{e_r^2 + (\frac{d}{dt}e_r)^2\right\} \geq 0.$$

Using (16) and (15), the derivative of $V_r$ with respect to time can be evaluated as follows, and it can be shown

that there exists a positive constant $B_2$:

$$\begin{aligned}\frac{d}{dt}V_r &= (k_1+\epsilon k_2)e_r\frac{d}{dt}e_r - \frac{d}{dt}e_r\left\{k_1e_r + k_2\frac{d}{dt}e_r\right\} \\ &\quad +\epsilon m(\frac{d}{dt}e_r)^2 - \epsilon e_r\{k_1e_r + k_2\frac{d}{dt}e_r\} \\ &\leq -B_2\{e_r^2 + (\frac{d}{dt}e_r)^2\} \\ &\leq -\frac{B_2}{B_1}V_r. \end{aligned} \quad (18)$$

(18) implies that the radius $r$ converges to the desired value $r_d$ exponentially as far as the input $\theta$ can be realized by (15).

Straight line case

Denote the reference straight line as $ax+by=c$, where $a$, $b$, and $c$ are the parameters of the line, and the control objective is such that the position of the UAV ($x_I$ and $y_I$) converges to this reference line. Define the error from the reference to the current position of the UAV as $e_l = ax_I + by_I - c$. Let $k_3$ and $k_4$ be positive constants. Assuming $a\sin\alpha - b\cos\alpha \neq 0$, the input $\theta$ is defined to satisfy

$$\sin\theta = \frac{-k_3e_l - k_4\frac{d}{dt}e_l - (T-D)(a\cos\alpha + b\sin\alpha)}{L(a\sin\alpha - b\cos\alpha)}, \quad (19)$$

as far as the right-hand side is within the range of $-1$ to 1; otherwise, $\theta$ will be selected to clip to $-\pi$ or $\pi$. The convergence of $e_l$ to 0 can be implied as follows.

Introducing a small positive constant $\mu$, a scalar function $V_l$ is defined as

$$V_l = \frac{k_3+\mu k_4}{2}e_l^2 + \frac{m}{2}\left\{\frac{d}{dt}e_l\right\}^2 + \mu m e_l\frac{d}{dt}e_l. \quad (20)$$

As shown in the circular reference case, if $\mu$ is sufficiently small, there exists a positive constant $C_1$ that holds to

$$V_l \geq C_1(e_l^2 + \left\{\frac{d}{dt}e_l\right\}^2) \geq 0. \quad (21)$$

Using (13), (14), and (19), the derivative of $V_l$ with respect to time can be evaluated as

$$\begin{aligned}\frac{d}{dt}V_l &= (k_3+\mu k_4)e_l\frac{d}{dt}e_l + \frac{d}{dt}e_l(a_1 + a_2\sin\theta) \\ &\quad +\mu m\left\{\frac{d}{dt}e_l\right\}^2 + \mu e_l(a_1 + a_2\sin\theta),\end{aligned}$$

where $a_1 = (T-D)(a\cos\alpha + b\sin\alpha)$ and $a_2 = L(a\sin\alpha - b\cos\alpha)$. Since $a_2\sin\theta = -a_1 - k_3e_l - k_4\frac{d}{dt}e_l$, there exists a positive constant $C_2$ that satisfies

$$\begin{aligned}\frac{d}{dt}V_l &\leq -C_2(e_l^2 + \left\{\frac{d}{dt}e_l\right\}^2) \\ &\leq -\frac{C_2}{C_1}V_l \leq 0, \end{aligned} \quad (22)$$

which proves the statement .

Input conversion

Although the path-following commands defined above are for the roll angles $\theta$ and yaw $\alpha_d$, it is necessary to convert those quantities to the reference quaternion in order to supply the information to the attitude controller. The reference quaternion is denoted as $\boldsymbol{q}_d$. Then, the following is used for the conversion:

$$\begin{aligned}\boldsymbol{q}_d &= \begin{bmatrix}\cos\frac{\alpha_d}{2}\\0\\0\\\sin\frac{\alpha_d}{2}\end{bmatrix}\odot\begin{bmatrix}1\\0\\0\\0\end{bmatrix}\odot\begin{bmatrix}\cos\frac{\theta}{2}\\\sin\frac{\theta}{2}\\0\\0\end{bmatrix} \\ &= \begin{bmatrix}\cos\frac{\theta}{2}\cos\frac{\alpha_d}{2}\\\sin\frac{\theta}{2}\cos\frac{\alpha_d}{2}\\\sin\frac{\theta}{2}\sin\frac{\alpha_d}{2}\\\cos\frac{\theta}{2}\sin\frac{\alpha_d}{2}\end{bmatrix}. \end{aligned} \quad (23)$$

## 4 Numerical simulation

In order to verify the proposed control scheme, the proposed method was tested through numerical simulations.

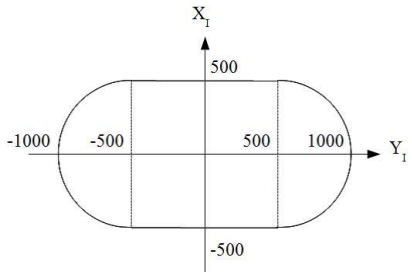


Figure 3: Reference path

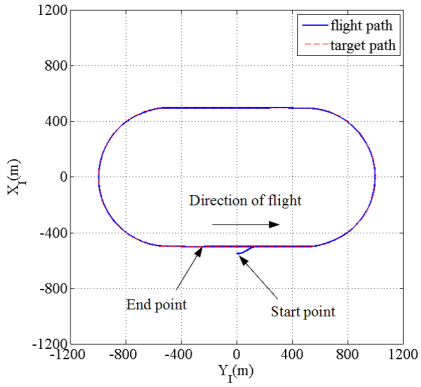


Figure 4: Flight path

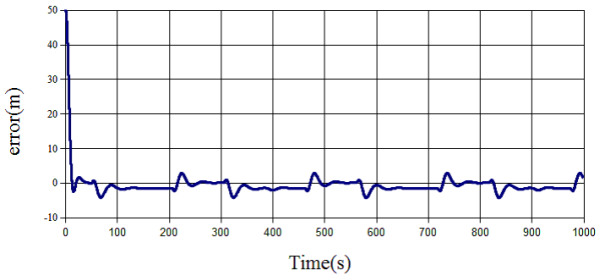


Figure 5: Path-following error

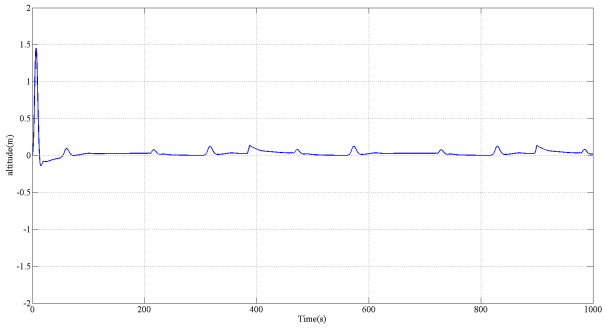


Figure 6: Altitude

### 4.1 Path-following guidance

The oval-like path with connecting arcs and line segments shown in Fig. 3 is considered as the reference path to follow. The UAV was located 50 m offset from the reference path at the initial state, but its direction was aligned with the path direction. The altitude at the initial state was the same as the reference.

The path followed by the UAV in the $x - y$ plane is shown in Fig. 4. The figure shows that the UAV converged to the desired path smoothly and tracked it well.

Figure 5 shows the path-following errors $e_l$ and $e_r$ with respect to time. The errors reached 0 exponentially and remained close to the origin, although they oscillated because the controller was derived based on the approximate model in this paper. Figure 6 shows the response of the altitude during the flight. It deviated at the initial transient period and converged back to the desired value 0. This quantity also fluctuated around the desired value, but it was also kept close enough to the reference.

Figure 7 and Fig. 8 show the attitude error in the quaternion and the euler angle. The real part deviated within the range of $(-0.05, 0.05)$, and the imaginary part elements were also maintained close to 0 throughout the flight, which validates that the attitude controller succeeded to track the reference roll and yaw angles generated by the outer-loop path-following mechanism.

As a comparison, the PID controller that utilized the error between the current position and the desired path was also tested (Fig. 9). It was not easy to tune the PID gains for both the straight reference segment and the circular curves simultaneously by considering the control surface saturation, and the achieved performance was poorer than the proposed method, as shown in the figure.

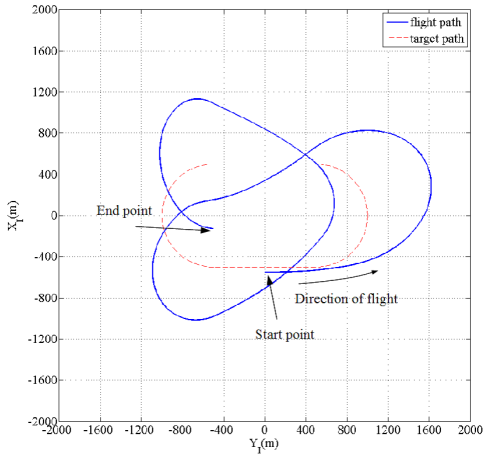


Figure 9: Flight path by PID control

### 4.2 Discussion

Although the proposed controller is developed based on a point mass and approximated dynamics for path following, and it is assumed that the attitude can be perfectly controlled by the inner loop in order to achieve path-following control, the above simulation showed that the UAV could follow the reference path almost perfectly, which validates the proposed approach. Oscillation close to the reference path might be able to be suppressed by tuning the feedback gain, but input saturation may reduce the performance, and the gain tuning process needs to be considered further. The noise in the measurement is not considered in this paper, and it may also deteriorate the performance.

## 5 Conclusion

This paper proposed a path-following control system based on nonlinear attitude control for a small UAV with a delta wing. Introducing simple point-mass dynamics, the stability of the path-following control system was considered, and the approach was validated through numerical simulations.

## References

Takuya Akasaka and Makoto Kumon. Robust attitude control system for kite plane. In *Proceedings of Sys-*

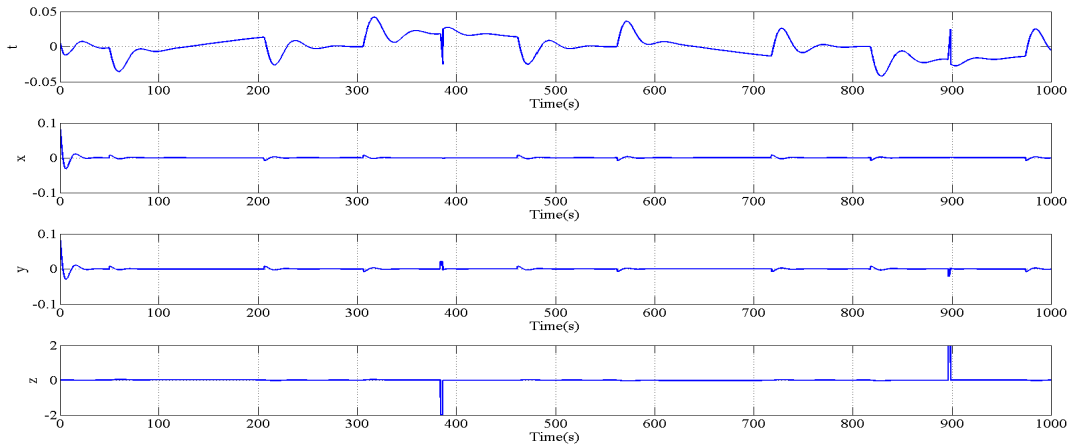


Figure 7: Quaternion error

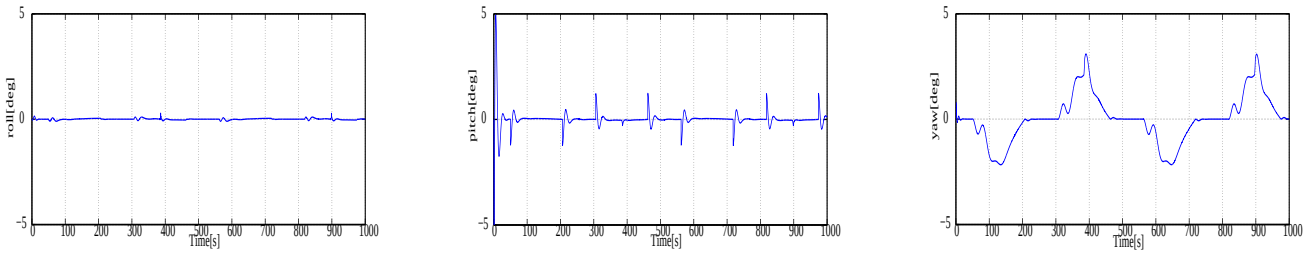


Roll Pitch Yaw

Figure 8: Attitude error in Euler angle

*tem Integration 2012*, pages 1623–1626, 2012. (in Japanese).

HaiYang Chao, YongCan Cao, and YangQuan Chen. Autopilots for small unmanned aerial vehicles: a survey. *International Journal of Control, Automation and Systems*, 8(1):36–44, 2010.

Lester E. Dubins. On curves of minimal length with a constraint on average curvature, and with prescribed initial and terminal positions and tangents. *American Journal of Mathematics*, 79(3):497–516, 1957.

Makoto Kumon, Yuya Udo, Hajime Michihira, Masanobu Nagata, Ikuro Mizumoto, and Zenta Iwai. Autopilot system for kiteplane. *IEEE/ASME Transactions on Mechatronics*, 11(5):615–624, oct 2006.

Th Mueller and James D DeLaurier. An overview of micro air vehicle aerodynamics. *Progress in Astronautics and Aeronautics*, 195:1–10, 2001.

R. M. Murray, Z. Li, and S. S. Sastry. *A Mathematical Introduction to Robotic Manipluation*. CRC Press, 1994.

Masanobu Nagata, Makoto Kumon, Ryuichi Kouzawa, Ikuro Mizumoto, and Zenta Iwai. Automatic flight path control of small unmanned aircraft with deltawing. In *Proc. of the Int. Conf. on Control, Automat. and Syst.*, pages 1383–1388, Bangkok, Thailand, August 2004.